

Modeling the Statistical Time and Angle of Arrival Characteristics of an Indoor Multipath Channel

Quentin H. Spencer, Brian D. Jeffs, Michael A. Jensen, A. Lee Swindlehurst
Department of Electrical & Computer Engineering
Brigham Young University
Provo, UT 84602

voice: (801) 378-7515
fax: (801) 378-6586
email: *spencerq@ee.byu.edu*

Keywords

indoor radio communications, radio propagation, communication channels, multipath channels

Abstract

Most previously proposed statistical models for the indoor multipath channel include only time of arrival characteristics. However, in order to use statistical models in simulating or analyzing the performance of systems employing spatial diversity combining, information about angle of arrival statistics is also required. Ideally, it would be desirable to characterize the full space-time nature of the channel. In this paper, a system is described that was used to collect simultaneous time and angle of arrival data at 7 GHz. Data processing methods are outlined, and results obtained from data taken in two different buildings are presented. Based on the results, a model is proposed that employs the clustered “double Poisson” time of arrival model proposed by Saleh and Valenzuela [1]. The observed angular distribution is also clustered, with uniformly distributed clusters, and arrivals within clusters that have a Laplacian distribution.

I. INTRODUCTION

Wideband digital wireless communications are becoming increasingly more practical in indoor environments. The availability of new frequency spectra in the 900 MHz, 2.4 GHz, and 5.7 GHz ranges are making wireless an attractive option for applications such as local area networks. Wireless networks can be particularly advantageous for applications which require portability, or where installation of wiring is undesirable or impractical.

One of the biggest obstacles to the more widespread use of wireless networks is the challenging indoor propagation environment, which leads to multipath with significant time

and angular spreading. To more fully understand indoor radio propagation, a number of researchers have collected data at frequencies commonly used in wireless networks, and attempted to develop models that fit their measurements. To date, most of these studies have focused on the temporal properties of the indoor channel.

Because of the rough similarity between the multipath channels in indoor and urban environments, early research in modeling indoor propagation was based on previous work involving urban multipath environments. A seminal paper in this area is that by Turin, et al [2], which was a basis for the comprehensive study of indoor propagation conducted by Saleh and Valenzuela [1]. Their model is based on a temporal clustering phenomenon they observed in their indoor multipath data. Other related models on indoor propagation have been developed more recently, such as that proposed by Ganesh and Pahlavan [3]. Their model is an extension of that in [2], a modified Poisson process where the probability of an arrival in a time bin is partially dependent on whether or not an arrival was observed in the previous time bin. Many others have addressed various aspects of the indoor channel, as reported, for example, in [4], [5], [6], [7], [8]. Various survey articles have recently appeared which have a large number of references on indoor propagation [9], [10], [11], and one discusses statistical channel modeling for both indoor and outdoor channels [12].

Until recently, the majority of research on indoor propagation has ignored the spatial aspect of the channel. Besides the fact that most indoor wireless networks were single-antenna systems, the issue of modeling the spatial characteristics of the channel had not been previously addressed due to the complexity of making such measurements. It is significantly more difficult to simultaneously collect space-time data than it is to make only time-domain impulse response measurements. However, as more consideration is given to multiple antenna systems that employ spatial diversity, the need for an accurate space-time model is clear.

The papers by Ganesh and Pahlavan [6] and Todd et al [7] were initial attempts at addressing the spatial aspects of indoor propagation. Both presented data that were collected with small variations in the location of the receiving antenna, and both also addressed the effects of the movement of people near the transmitting and receiving antennas. Early research that specifically addressed the angle of arrival is found in [13], [14], [15] and [16]. More recently, research has begun to focus on statistical channel models that include both time and angle

of arrival [17], [18], though as yet no space-time channel models based on measured channel responses have been developed.

The goal of this paper is to undertake a more comprehensive study of the joint temporal and spatial properties of the indoor propagation environment. We have assembled a data acquisition system that is capable of resolving multipath arrivals simultaneously in space and time with a resolution of 6° and 3 ns, respectively. The system was used to collect a number of data sets from two different buildings on the Brigham Young University (BYU) campus. This paper reports the results of these measurements, and based on them proposes a statistical model for both the spatial and temporal components of the indoor channel. Multipath clustering in time similar to that described in [1] was observed in our data, and so we employ the temporal description of the data used in [1] in our joint model. In addition, clusters of arrivals were also found to exist in angle, and the distribution of the individual clusters was found to be approximately Laplacian. Another key observation from our data is that, on average, the temporal and spatial channel parameters appear to be independent of one another.

Since the space-time model we propose in this paper is an extension of the time-only model of [1], we begin in the next section with a brief discussion of this approach, and continue in Section III with a description of the proposed joint space-time model based on the Saleh-Valenzuela model. Section IV contains a description of the hardware setup used to collect the indoor data studied herein, and Section V presents the techniques used to extract time and angle of arrival information from the data. Section VI is a discussion of the results and model parameters extracted from the data. The paper concludes with a summary of results and some topics for further research.

II. THE SALEH-VALENZUELA MULTIPATH PROPAGATION MODEL

The model of Saleh and Valenzuela [1] closely reflects the characteristics of the data presented here, and thus is used as a basis for the extended model. This section summarizes the most important aspects of their model. The model is based on a clustering phenomenon observed in their experimental data. In all of their observations, the arrivals came in one or two large groups within a 200 ns observation window. It was observed that the second

clusters were attenuated in amplitude, and that rays, or arrivals within a single cluster, also had amplitudes that decayed on average with time. Their model proposes that both of these decaying patterns are exponential with time, and are controlled by two time constants: Γ , the cluster arrival decay time constant, and γ , the ray arrival decay time constant. Figure 1 illustrates this, showing the mean envelope of a three cluster channel.

The impulse response of the channel they considered is given by:

$$h(t) = \sum_{l=0}^{\infty} \sum_{k=0}^{\infty} \beta_{kl} e^{j\phi_{kl}} \delta(t - T_l - \tau_{kl}), \quad (1)$$

where the sum over l represents the clusters, and the sum over k represents the arrivals within each cluster. The $e^{j\phi_{kl}}$ term represents a statistically independent random phase associated with each arrival, where ϕ_{kl} is uniform on $[0, 2\pi)$. The total time delay of each arrival is the sum of T_l , the delay of the l th cluster, and τ_{kl} , the delay of the k th arrival in the l th cluster. The amplitude of each arrival is given by β_{kl} , which is assumed to be a Rayleigh distributed random variable whose mean square value is described by the double-exponential decay illustrated in Figure 1. This mean squared value is modeled by:

$$\overline{\beta_{kl}^2} = \overline{\beta^2(T_l, \tau_{kl})} \quad (2)$$

$$= \overline{\beta^2(0, 0)} e^{-T_l/\Gamma} e^{-\tau_{kl}/\gamma}, \quad (3)$$

where $\overline{\beta^2(0, 0)}$ is the average power of the first arrival of the first cluster. This average power is a function of the distance separating the transmitter and receiver.

The time of arrival is described by two Poisson processes which model the cluster arrival times and the arrival times of rays within clusters. The time of arrival of each cluster is an exponentially distributed random variable conditioned on the time of arrival of the previous cluster. The case is the same for each ray, or arrival within a cluster. Following the terminology used in [1], *rays* shall refer to arrivals within clusters, so that the term *cluster arrival rate* denotes the parameter for the intercluster arrival times, (Λ), and the *ray arrival rate* refers to the parameter for the intracluster arrival times, (λ). The distributions of these arrival times are shown in equations (4) and (5):

$$p(T_l | T_{l-1}) = \Lambda e^{-\Lambda(T_l - T_{l-1})}, \quad T_{l-1} < T_l < \infty \quad (4)$$

$$p(\tau_{kl} | \tau_{(k-1)l}) = \lambda e^{-\lambda(\tau_{kl} - \tau_{(k-1)l})}, \quad \tau_{(k-1)l} < \tau_{kl} < \infty. \quad (5)$$

These two distributions are assumed to be independent of each other. Furthermore, T_0 and τ_{0l} are both assumed to be zero. This implies that all times are relative with respect to the bulk delay of the first arrival.

In [1], the parameters Γ and γ were estimated by superimposing clusters with normalized amplitudes and time delays and selecting a mean decay rate. The estimated parameters from their data were $\Gamma = 60$ ns and $\gamma = 20$ ns. The Poisson cluster arrival rate parameter, Λ , was estimated so that the probabilities of the total number of clusters per random channel closely matched the statistics of the observed data. This produced an estimate of $1/\Lambda \approx 300$ ns. The ray arrival rate parameter was approximated based on the average separation time between arrivals. The estimate for their data was $1/\lambda \approx 5$ ns. As their data did not provide spatial information, angle of arrival was not addressed in [1].

III. A COMBINED TEMPORAL/SPATIAL STATISTICAL MODEL FOR INDOOR MULTIPATH PROPAGATION

A. Time of Arrival

In this section we propose a statistical model for the indoor multipath channel that includes a modified version of the Saleh-Valenzuela time-of-arrival model, and incorporates spatial information. This model is based on a collection of space-time channel measurements that will be described in Sections IV-VI.

As in [1], we assume that the time delay and amplitude component of the combined model is represented by $h(t)$ in equation (1), where, as before, $\overline{\beta_{kl}^2}$ is the mean square value of the k th arrival of the l th cluster. This mean square value is described by the exponential decay given in equation (3) and illustrated in Figure 1. As before, the ray arrival time within a cluster is assumed to be described by the Poisson process of equation (5), and the time delay of the first arrival in each cluster is denoted by T_l , described by the Poisson process of (4). The inter-ray arrival times, τ_{kl} , are dependent on the time of the first arrival in the cluster T_l . In the Saleh-Valenzuela model, the first cluster arrival time T_0 was assumed to be zero, implying that all times T_l are measured relative to the bulk delay of the first arrival.

B. Angle of Arrival

The data collected for this paper show that arrivals tended to be clustered in both time and angle. Therefore, in addition to the cluster and ray arrival times T_k and τ_{kl} , we propose that the angle of arrival be characterized by a cluster angle (Θ_l) and a ray angle (ω_{kl}). This results in the addition of an angle-of-arrival term to the channel impulse response given in (1). The combined impulse response is thus taken to be:

$$h(t, \theta) = \sum_{l=0}^{\infty} \sum_{k=0}^{\infty} \beta_{kl} e^{j\phi_{kl}} \delta(t - T_l - \tau_{kl}) \delta(\theta - \Theta_l - \omega_{kl}), \quad (6)$$

The time-only model assumed the cluster times T_l to be statistically independent of the ray times τ_{kl} . Likewise, we will assume that the cluster statistics (the distributions of T_l and Θ_l) are independent of the ray statistics (distributions of τ_{kl} and ω_{kl}).

Similar to the time-of-arrival model, all angles are measured with respect to the angle of the first cluster, Θ_0 . The time and angle of the first arrival are heavily dependent on the specific room geometry, and all measurements are made with respect to it in order to eliminate these effects. The data presented here show that the conditional distribution of Θ_l given Θ_0 (or $p(\Theta_l|\Theta_0)$) is approximately uniform on $[0, 2\pi)$. The cluster arrival angles Θ_l are not meant to be the angle of the first arrival within a cluster, but the mean of all angles of arrival for the cluster. Thus the distribution of the ray arrival angle, ω_{kl} , has a zero mean. Based on the data presented later, we propose a zero-mean Laplacian distribution with standard deviation σ :

$$p(\omega_{kl}) = \frac{1}{\sqrt{2}\sigma} e^{-|\sqrt{2}\omega_{kl}/\sigma|}. \quad (7)$$

The suitability of these distributions in accurately modeling the channel will be discussed later.

C. Correlation of Time and Angle

As already mentioned, the cluster statistics and ray statistics are assumed to be independent, but with the introduction of angle of arrival into the model there is the potential of a correlation between time and angle. If the time and angle distributions are independent,

the cluster and ray statistics are separable functions:

$$p(T_l, \Theta_l | T_{l-1}, \Theta_0) = p(T_l | T_{l-1})p(\Theta_l | \Theta_0) \quad (8)$$

$$p(\tau_{kl}, \omega_{kl} | \tau_{(k-1)l}) = p(\tau_{kl} | \tau_{(k-1)l})p(\omega_{kl}) \quad (9)$$

For the sake of simplicity, and based on our data, we assume that these distributions are indeed independent. The reasons for this conclusion will be discussed later.

IV. DATA ACQUISITION SYSTEM

The basic technique used to collect the data involved pointing an antenna with a narrow angular resolution in a certain direction, measuring the time domain impulse response of the channel in that direction, rotating the antenna a small amount, and repeating the procedure until full 360° coverage was obtained. A Hewlett-Packard 8720B network analyzer was used as a signal generator and receiver. The transmitted signal was sent from the network analyzer to the transmitting antenna through a low-loss 36 m coaxial cable. A chirp signal of 500 MHz bandwidth was transmitted, resulting in an effective pulsewidth of approximately 3 ns. A block diagram of the system is shown in Figure 2. The data produced by this setup can best be viewed in the form of an image plot of received power with respect to time and angle. An example of this is shown in Figure 3. In this figure, and in the others like it, delay represents absolute delay from the transmitter with a 25 ns offset.

The frequency band used for our experiments was 6.75 to 7.25 GHz. To date, this particular frequency range has not been the subject of much study for indoor applications; its selection for our work was due primarily to the availability of the required hardware. However, the apparent trend toward increasingly higher frequencies for indoor wireless (as high as 60 GHz in one paper [14]), and recent frequency allocations in the United States between 5 and 6 GHz for use in wireless local area networks makes this choice of frequency very relevant.

The data were gathered during regular daytime working hours, and in some cases there were people moving in the rooms where the data were collected. This had very little effect on the data, because multiple measurements were taken for each angle and the results averaged. This offset the effects of any non-stationarity in the channel, and also improved the overall signal to noise ratio of the data.

The antenna used in the data acquisition system was a dish antenna with a diameter of 60 cm. At a frequency of 7 GHz, the antenna has a 3 dB beam width of about 6° in both the horizontal and vertical directions, and a null-to-null beam width of roughly 10° . It is anticipated that most of the received energy from the channel will be confined to the horizontal plane (assuming both the transmit and receive antennas are, say, on the same floor of a given building), but it is possible that there are multipath components with significant vertical displacement. For this reason, the narrow vertical beam width of the antenna may provide incomplete information about the channel in question. To test this, the antenna was temporarily modified to increase the vertical 3 dB beam width to approximately 30° . A comparison of the results from the modified and unmodified antenna, shown in Figure 4, revealed that while the relative amplitudes of the major arrivals had changed, the general clustering structure was unchanged. Thus, for purposes of obtaining a statistical model, the antenna was left unmodified for data collection, since the modification caused a loss of about 5 dB.

V. DATA PROCESSING AND ANALYSIS

A. Image Processing

Although diffuse multipath components are visible in the images of Figures 3, most of the energy is highly localized in space and time. Consequently, we choose to model only the specular component of the multipath channel. As such, the images shown above can be modeled as a collection of point sources blurred by a point spread function (PSF) and corrupted by additive noise. This assumption reduces the problem of identifying exact times and angles of arrival to one of 2-D deconvolution, which would normally be very difficult in the diffuse source (or scattering) case.

The PSF or impulse response of the system was generated by setting up the data acquisition system in a line of sight environment with a high signal to noise ratio and no reflections in the vicinity of the direct path. Sidelobes along the angular axis result from the beam pattern of the antenna, while sidelobes in time result from the effects of windowing and pulse shaping. Because the point spread function is known with reasonable accuracy, the deconvolution problem lends itself well to the CLEAN algorithm [19]. The CLEAN algorithm was

originally used for processing astronomical images, which are also often modeled as groups of point sources convolved with a blurring function. The algorithm is essentially a recursive subtraction of the PSF from the image, with the PSF positioned to correspond with the maximum value of the image. The highest peak is found, its amplitude, time, and angle are stored, and a scaled copy of the impulse response is subtracted from the image. This process is repeated on the residual image until a predetermined threshold (usually corresponding to the noise level) is reached.

One difficulty with the CLEAN algorithm is that slight misalignments in the estimated position of the PSF center can lead to artifacts, or points that are taken as arrivals where obviously none are present. Furthermore, around very strong arrivals, the surrounding areas tend to be significantly stronger than the noise floor. This combined with the PSF model error in the side lobes could cause many points in those areas to be interpreted as arrivals. Other sources of false detections may include volume reverberation or multiplicative noise in the system.

To combat this problem, a scheme known as constant false alarm rate detection was used [20]. The noise floor threshold was adjusted at each point based on the average power of the surrounding samples within a certain window. This greatly reduced the number of false arrivals that were detected, but did not eliminate them all. While a manual search or a more complex algorithm could have been used, the CLEAN algorithm with constant false alarm level detection proved to be the simplest and overall the most reliable means of accurately identifying the location of the major multipaths.

B. Cluster Finding

The result of the deconvolution process is shown by the x's superimposed on Figure 3. In order to analyze the statistics of clustering effects, the next task was to identify the presence and composition of any clusters in the data. Early analysis of the data showed clustering effects in both time and angle. These clusters were obvious to the observer in most cases. Some experimentation was done with computer algorithms for automatic cluster identification, but eventually it was decided that the overall amount of data was small enough that the clusters could easily and accurately be determined manually. This was done via

a computer program that displayed an image of the processed data, and allowed the user to identify clusters using graphical input, similar in concept to the process used by Saleh and Valenzuela, who also identified clusters by visual observation. With the times, angles, amplitudes, and clusters of all major arrivals identified, the data could be used to analyze the channel statistics and arrive at a model.

VI. RESULTS

This section presents some comparisons between the proposed model and the data that were obtained using the collection system described earlier. Data were collected in two buildings of significantly different construction. The two buildings studied are representative of the steel and concrete frame buildings common in institutional and commercial settings. In all of the collection scenarios, the transmitter and receiver were separated by a wall, and in most cases they were in different rooms. Separation distances ranged from approximately 6 to 30 meters. Most doors in both buildings were made of wood, and were closed for all measurements. The following sections discuss general trends observed in the data, and the model parameters derived from the data for the two buildings.

A. General Observations

A total of 55 data sets were recorded on the fourth floor of the Clyde Building (CB) on the Brigham Young University campus, and another 10 data sets were collected in the Crabtree Building (CTB), a newer building also located on the BYU campus. The CB is constructed mostly of reinforced concrete and cinder block, with all internal walls composed of cinder block. The building Saleh and Valenzuela used for their measurements is similar in construction to the CB. The CTB is built with steel girders, and internal walls are gypsum board over a steel frame. The model parameters estimated from the experimental data for each building are discussed below.

As alluded to earlier, a clustering pattern in angle was immediately visible in the processed data images. Generally there were at least two or three clusters, except in rare cases with long propagation distances and consequently low signal-to-noise ratios. There were some extreme cases of more than five clusters, especially in the CTB data. The average number of

clusters per data set in the CTB was about 5, while for the CB the average was 3. Histograms of the number of clusters for each building are shown in Figure 6.

In general, fewer clusters were observed when the transmitter/receiver separation was large due to the correspondingly lower signal-to-noise ratio (SNR). A higher number of clusters occurred with a stronger signal when the channel possessed a more complex geometry; i.e. more doorways, walls, or rooms in between the transmitter and receiver. The higher overall number of clusters in the CTB seems to be a result of the fact that the building's construction produced more reflections and attenuated the signals less, and hence more long-delay arrivals could be seen. As documented in the next section, clusters were observed at all angles. In most clusters, the majority of arrivals were located within 20 to 30 degrees of the cluster mean, with occasional outliers.

In both buildings, the line of sight (LOS) path was almost always present in the data, but its level of attenuation was dependent on the number and type of walls between the transmitter and receiver (LOS was observed in cases of up to 3 walls). In the CTB the LOS component was stronger than in the CB. In both buildings, when there was only a single wall separating the transmitter and receiver, the LOS arrival was generally the strongest. It appeared that almost all door openings provided a non-LOS cluster, even with the doors closed. Almost all strong clusters had a corresponding cluster that appeared to be a back-wall reflection. However, the relative angles of the back-wall reflections tended to vary with the geometry of the specific situation. For example, a receive location near a corner can produce two strong back-wall reflections from each of the nearby walls, but the angles can vary widely depending on transmitter location.

In most respects, the data collected in the two buildings did not differ greatly. Both data sets exhibited similar clustering structures, as well as a decay over time of the amplitudes of the clusters and the rays within clusters. The most pronounced difference was a much slower decay rate in the CTB data, which produced a corresponding increase in the total number of arrivals, and a slight increase in the number of clusters. The next two sections present the specific model parameter estimates for the CB and CTB.

B. Clyde Building

The cluster and ray decay time constants, Γ and γ , were estimated using the same method as in [1]. The first cluster arrival in each set was normalized to an amplitude of 1 and a time delay of 0. All arrivals were superimposed and plotted on a semilogarithmic plot as shown in Figure 7. The estimate for Γ was found via a least-squares fit of the data to an exponential curve. For the CB, Γ was found to be 34 ns, which is slightly more than half the figure found in [1], where it was estimated to be 60 ns.

Figure 8 shows the data and estimated curve for γ obtained using the same method. The first arrival in each cluster was set to a time delay of zero and an amplitude of one, and all other arrivals were then adjusted accordingly and superimposed. The superimposed curve represents $\gamma = 29$ ns, which is quite close to the value of 30 ns found in [1].

It is obvious from the large variance of the amplitudes at each delay that the assumption of exponential decay can only reflect the mean behavior of the channel. In their data, Saleh and Valenzuela did not have information about the specific time and amplitude of arrival that was as accurate as that presented here. As a result, they made rough estimates for the amplitude decay parameters and did not attempt to generate plots like Figure 7 or 8. However, in their case, as well as with this data, the general trend is a linear decline of log-amplitude over time, indicating that to first order at least, the amplitude decay is exponential.

It can be seen in Figures 7, 8, that the first arrival was not always the strongest arrival, which is likely due to occasional sidelobes or noise being taken as an arrival by the CLEAN algorithm. Because of this fact, the amplitude of the curve at zero delay was allowed to vary from the standard value of one when finding the best fit. This allowed for a curve which better followed the general decay trend of the data.

The rate-of-arrival parameters were easily estimated from the data since the precise time of arrival was known for each ray and cluster. To estimate Λ , the cluster arrival rate, the first arrival in each cluster was considered to be the beginning of the cluster, regardless of whether or not it had the largest amplitude. The arrival time of each cluster was subtracted from that of its immediate predecessor, so that the delay parameter of the conditional probability distribution given in (4) could be determined. Estimates for both Λ and λ were obtained by

a least-squares fit of the sample probability density function to the measured probabilities for each bin. Figure 9 shows this cumulative density function on a log scale and the closest exponential fit. This data does not include the first arrival in each data set, for reasons that will be discussed in the next section. In this case $1/\Lambda = 17$ ns. The possible reasons for the large discrepancy between this estimate and the estimate of 300 ns given in [1] will also be discussed at the end of this section.

The second Poisson parameter, λ , representing the ray arrival rate, was estimated in a similar fashion. Each within-cluster time-of-arrival was subtracted from the previous one to produce a set of conditional arrival times $p(\tau_{kl}|\tau_{(k-1)l})$. The cumulative distribution of these with the best fitting pdf is shown in Figure 10. In this case, $1/\lambda = 5$ ns.

Figure 11 shows a CDF of the mean angle of each of the clusters. Each arrival angle plotted is measured relative to the absolute angle of the first arrival in the data set. The distribution looks very uniform, except that the interval between 50° and 310° (about 50° on each side of zero) contains very few arrivals (also visible in Figure 5). The explanation for this is simply that arrivals near the reference cluster are likely classified as belonging to that cluster. The results shown here support the conclusion that the mean cluster angles are distributed uniformly over all angles.

The distribution of the ray arrivals with respect to the cluster mean is shown in Figure 12. The characteristic sharp peak of the Laplacian distribution is immediately obvious. The superimposed curve is a Laplacian distribution that was fit by integrating a Laplacian PDF over each bin, and matching the curves using least squares. The Laplacian distribution turns out to be a very close fit. In this case the angular variance σ was measured to be 26° . The tail behavior of the distribution was examined by looking at the distribution on a log scale, and it was observed that the tails are actually heavier than predicted by a Laplacian distribution, but the model accurately captures the behavior of 90% of the arrivals.

C. Crabtree Building

The model parameters were evaluated for the CTB in the same way as they were for the Clyde Building, and the associated plots can be found in [21]. In general the fits were not quite as good because of the lower number of samples, but the data was useful for a

comparison with the Clyde Building results. The estimate for Γ was determined to be 78 ns, more than double the number found for the CB, but closer to the figure of 60 ns found in [1]. The most significant difference found in the CTB data was that the ray decay rate γ was found to be 82 ns, slower than the cluster decay rate Γ . The value of $1/\Lambda = 17$ ns is the same as the value measured for the CB, although the higher total number of clusters in the CTB indicates that this particular method of estimating Λ may give results that are low. The estimate of 7 ns for $1/\lambda$ is slightly slower than the estimate for the CB. The cluster angles of arrival conditioned on the first arrival in this case was also found to be quite uniform, as was the case in the CB. The ray angle of arrival also fit the proposed Laplacian distribution very well, with $\sigma = 22^\circ$. In this case, a log plot revealed that the Laplacian distribution accurately fit the tails of the distribution, demonstrating that the model accurately predicts the angular distribution in nearly 99% of the trials.

D. Correlation of Time and Angle

The time-space channel model proposed earlier makes the assumption that the statistics for the time and angle of the clusters and rays are independent, i.e. that $p(T, \Theta)$ and $p(\tau, \omega)$ are separable functions. In order to test this assumption on the data, 2-D scatter plots were generated as shown in Figure 5. The first plot is of the relative delays and angles of all clusters with respect to the first cluster. The second is a plot of the relative delay and angle of each ray with respect to the first cluster arrival time and the mean cluster arrival angle. The plots show that there is not a significant correlation between time and angle in either case. This is evident in the fact that the density functions appear to be approximately separable in both cases, and that there are rays or clusters present at nearly all times and angles. Based on this evidence, and for the sake of simplicity, we will assume that arrival times and angles are independent. However, these assumptions are based on a very small data set, and it is possible that a larger set of data could reveal some correlation.

E. Comparison of Model Parameters

Table I shows a comparison of the model parameters estimated for the CB, the CTB, and those presented in [1]. The most obvious discrepancy is in the estimates for the value of

parameter	Clyde Building	Crabtree Building	Saleh-Valenzuela
Γ	34 ns	78 ns	60 ns
γ	29 ns	82 ns	20 ns
$1/\Lambda$	17 ns	17 ns	300 ns
$1/\lambda$	5 ns	7 ns	5 ns
σ	26°	22°	—

TABLE I

A COMPARISON OF MODEL PARAMETERS FOR THE TWO BUILDINGS AND FROM SALEH AND VALENZUELA.

Λ . The explanation for this is quite straightforward. There were significantly more clusters observed in both the CB and CTB data compared with the average of 1-2 clusters observed in [1]. This may be due in part to the higher RF frequency used in our experiments. More significant, however, was the ability of our testbed to see clusters that overlapped in time, but were separated in angle. In many cases, clusters that would have been classified as a single group if observed only in time were clearly disjoint in space.

The values for λ for the various data sets were all very similar. The most interesting observation concerning the estimates of the amplitude decay parameters is that $\Gamma \simeq \gamma$ for both the CB and the CTB, unlike the results of [1]. The value of Γ was unusually low in the CB, while the value of γ for the CTB was especially unusual since it was not only large, but larger than the corresponding Γ . The likely explanation for this is that the walls in the CTB both reflect more (due to steel framing) and attenuate less (due to thin gypsum board coverings). The CB, which is similar in construction to the building used by Saleh and Valenzuela for their data, tended to have a higher attenuation, most likely due to the higher frequency used in our experiments. Both values of σ were close to each other, but there is no precedent that allows for comparison of this figure with other researchers' data.

F. Possible Causes for Various Aspects of the Model

Many aspects of the model have plausible physical explanations which we may propose as causes for the observed behavior. Because an absolute angular reference was maintained during the collection of the data, it was possible to compare the processed data with the geometry of each configuration. It was observed that the strongest cluster was almost always

associated with the LOS between the receiver and transmitter. This was true even though the LOS signal had to propagate through walls. The apparent causes of weaker clusters were back wall reflections and the presence of doorway openings, even when the doors were closed. Evidence of propagation through closed doorways was not surprising since all of the doors in the two buildings tested were composed of wood and were surrounded by metal frames. Such clusters would likely not be present in a building with metal doors.

A cluster with a narrow angular variance was centered at most doorway openings, likely accounting for the sharp peak in the Laplacian angular distribution. The location of the line of sight and the back wall reflection is very dependent on the specific arrangement of transmitter and receiver, and therefore, over a large number of rooms and locations, a uniform distribution of clusters in angle is reasonable.

The physical reasons for multipath clustering in the indoor environment seem to imply that there should be a stronger correlation between time and angle of arrival than was observed. For example, one might expect that as clusters diverge in angle from the line of sight, there should be a corresponding increase in the time delay of those clusters. This could also be said for the arrivals within clusters. However, our empirical analysis of the data did not give any significant evidence of such patterns. Because of the wide range of separation distances and room types used for this data, the model represents the mean behavior of the indoor channels tested. It is possible that data collected with narrower range of parameters may give additional insight into possible time/angle correlation.

VII. SUMMARY

Using a data collection system that took measurements in both space and time, information was obtained about the clustering structure of indoor wireless multipath signals, the angular distribution of these multipaths, and the behavior of multipath signals in buildings of varying structure. A definite clustering pattern was observed in the time-angle indoor multipath data. The temporal clustering observed in [1] is supported by the data presented here, and a clustering pattern in angle was also observed. The mean angles of each cluster were found to be distributed uniformly over all angles. The distribution of arrivals within clusters was approximately Laplacian, with standard deviations (angular spreads) ranging from 22° to

26°.

In general, the data presented here exhibited the same general characteristics as the Saleh-Valenzuela data. The amplitudes of clusters and rays within clusters both approximately follow a pattern of exponential decay, and the times of arrival in the data closely follow the model of [1]. There were some differences observed in the measured model parameters, most noticeably in the time decay rates. The other major discrepancy is in the markedly faster cluster arrival rate, which is most likely explained by the larger overall number of observed clusters resulting from a more sensitive data gathering apparatus.

The model parameters for the two buildings had more in common with each other than they did with those in [1]. Both buildings had similar parameters for angular distribution and rate of arrival, differing mainly in the amplitude decay parameters. The slower decay rates seen in the Crabtree Building are most likely due to the steel and gypsum construction of the building, which tends to both enhance reflections and reduce attenuation at the same time. In general, the model seemed to be able to accurately describe the differing multipath characteristics in both buildings, regardless of their very different construction. This implies that the model could possibly provide a general representation for many different types of buildings, and model parameters could then be found for buildings of varying construction.

REFERENCES

- [1] Adel A. M. Saleh and Reinaldo A. Valenzuela. A statistical model for indoor multipath propagation. *IEEE Journal on Selected Areas of Communications*, SAC-5:128–133, February 1987.
- [2] George L. Turin et al. A statistical model of urban multipath propagation. *IEEE Transactions on Vehicular Technology*, VT-21(1):1–9, February 1972.
- [3] R. Ganesh and K. Pahlavan. Statistical modeling and computer simulation of indoor radio channel. *IEE Proceedings-I*, 138(3):153–161, June 1991.
- [4] Robert J. C. Bultitude, Samy A. Mahmoud, and William A. Sullivan. A comparison of indoor radio propagation characteristics at 910 mhz and 1.75 ghz. *IEEE Journal on Selected Areas in Communications*, 7(1):20–30, January 1989.
- [5] Yuqiang Tang and Harold Sobol. Measurements of pcs microwave propagation in buildings. *Applied Microwave & Wireless*, pages 38–60, Winter 1995.
- [6] R Ganesh and K. Pahlavan. Statistics of short time and spatial variations measured in wideband indoor radio channels. *IEE Proceedings-H*, 140(4):297–302, August 1993.
- [7] Stephen R. Todd, Mohammed S. El-Tanany, and Samy A. Mahmoud. Space and frequency diversity measurements of the 1.7 ghz indoor radio channel using a four-branch receiver. *IEEE Transactions on Vehicular Technology*, 41(3):312–320, August 1992.
- [8] Theodore S. Rappaport and Dwayne A. Hawbaker. Wide-band microwave propagation parameters using circular and linear polarized antennas for indoor wireless channels. *IEEE Transactions on Communications*, 40(2):240–245, February 1992.
- [9] Jorgen Bach Andersen, Theodore S. Rappaport, and Susumu Yoshida. Propagation measurements and models for wireless communications channels. *IEEE Communications Magazine*, 33:42–49, January 1995.
- [10] D. Moltdar. Review on radio propagation into and within buildings. *IEE Proceedings-H*, 138(1):61–73, February 1991.
- [11] Homayoun Hashemi. The indoor radio propagation channel. *Proceedings of the IEEE*, 81:941–968, July 1993.

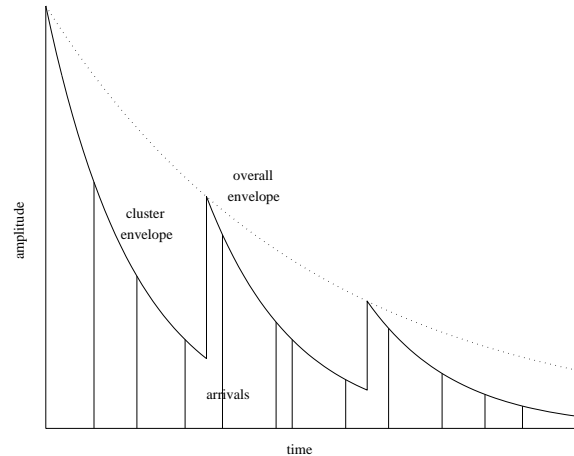


Fig. 1. An illustration of exponential decay of mean cluster power and ray power within clusters.

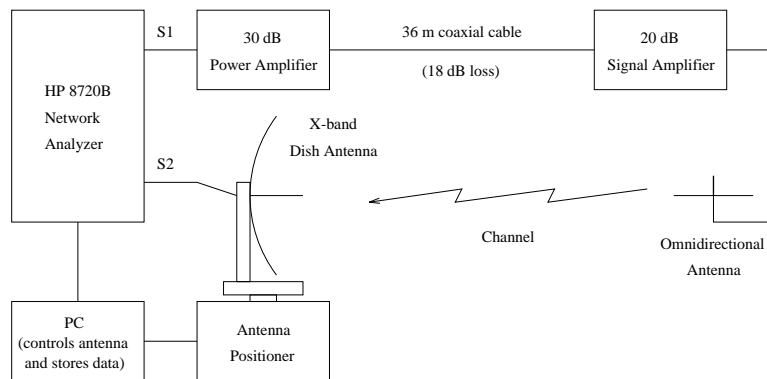


Fig. 2. The Data Acquisition System

- [12] Richard B. Ertel, Paulo Cardieri, Kevin W. Sowerby, Theodore S. Rappaport, and Jeffrey H. Reed. Overview of spatial channel models for antenna array communication systems. *IEEE Personal Communications*, pages 10–22, February 1998.
- [13] T. Lo and J. Litva. Angles of arrival of indoor multipath. *Electronics Letters*, 28(18):1687–1689, August 27 1992.
- [14] Jian-Guo Wang, Ananda S. Mohan, and Tim A Aubrey. Angles-of-arrival of multipath signals in indoor environments. In *IEEE Vehicular Technology Conference*, pages 155–159. IEEE, 1996.
- [15] Stephane Guerin. Indoor wideband and narrowband propagation measurements around 60.5 ghz. in an empty and furnished room. In *IEEE Vehicular Technology Conference*, pages 160–164, 1996.
- [16] John Litva, Amir Ghaforian, and Vytas Kezys. High-resolution measurements of aoa and time-delay for characterizing indoor propagation environments. In *IEEE Antennas and Propagation Society International Symposium 1996 Digest*, volume 2, pages 1490–1493. IEEE, 1996.
- [17] R. Heddergott, B. H. Fleury, and U. P. Bernhard. Stochastic radio channel model for advanced indoor mobile communication systems. In *IEEE International Symposium on Personal, Indoor, and Mobile Radio Communications*. IEEE, 1997.
- [18] Thomas Zwick, Christian Fischer, and Werner Wiesbeck. A statistical channel model for indoor environments including angle of arrival. In *IEEE Vehicular Technology Conference*. IEEE, 1998.
- [19] J. A. Högbom. Aperture synthesis with a non-regular distribution of interferometer baselines. *Astronomy and Astrophysics Supplement*, 15:417, 1974.
- [20] H. L. Van Trees. *Detection, Estimation, and Modulation Theory*. John Wiley and Sons, 1971.
- [21] Quentin H. Spencer. Modeling the statistical time and angle of arrival characteristics of an indoor multipath channel. Master’s thesis, Brigham Young University, November 1996.

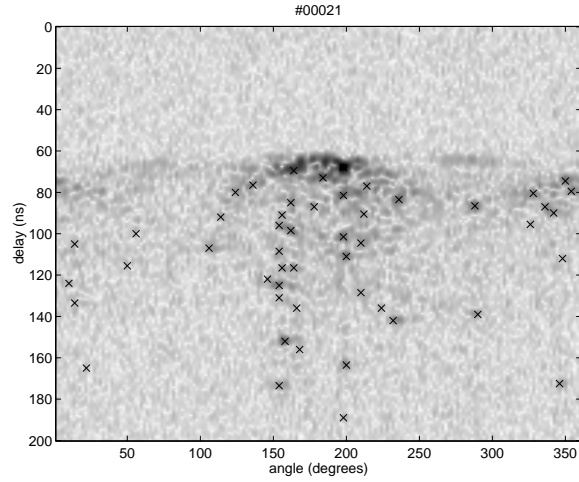


Fig. 3. Example of a raw data set. The processed data is superimposed.

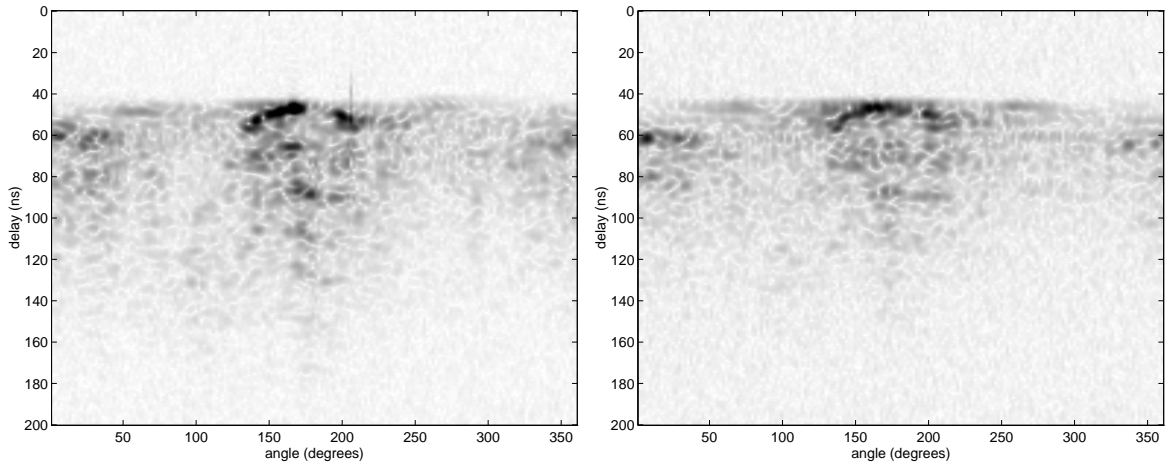


Fig. 4. Data Collected with Original Antenna (left), and with Modified Antenna (right).

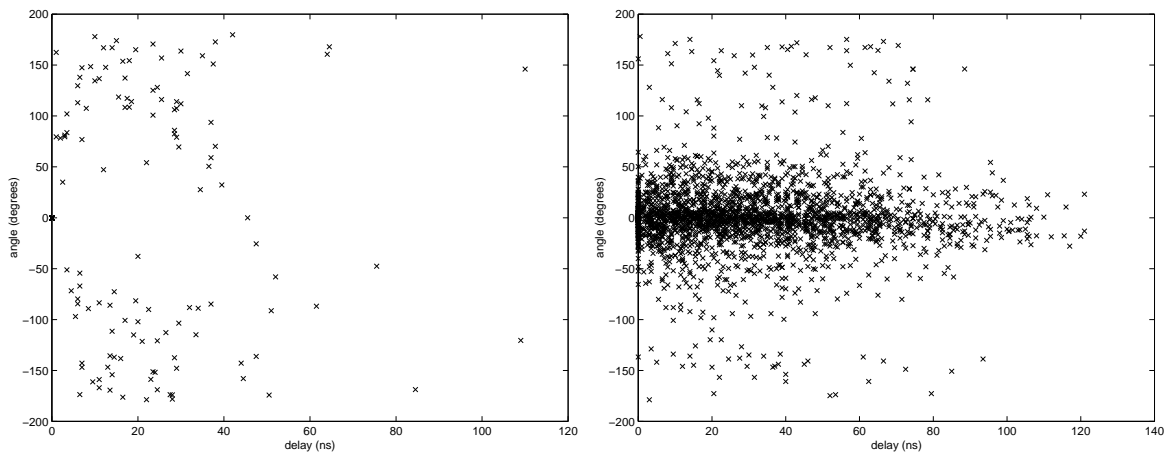


Fig. 5. Scatter plot of time and angle for clusters (left), and arrivals within clusters (right).

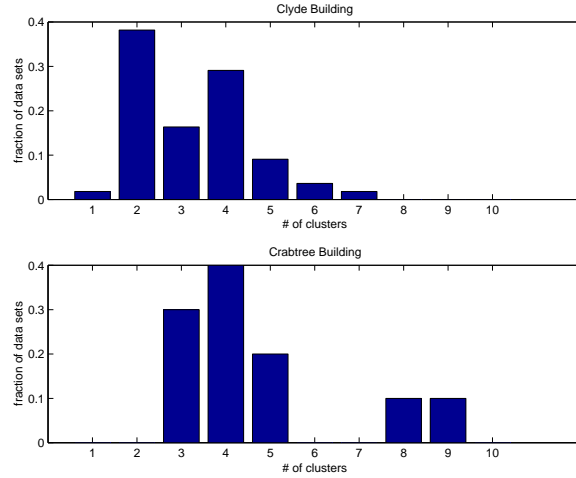


Fig. 6. Histogram of Number of Clusters per Location for the CB and CTB.

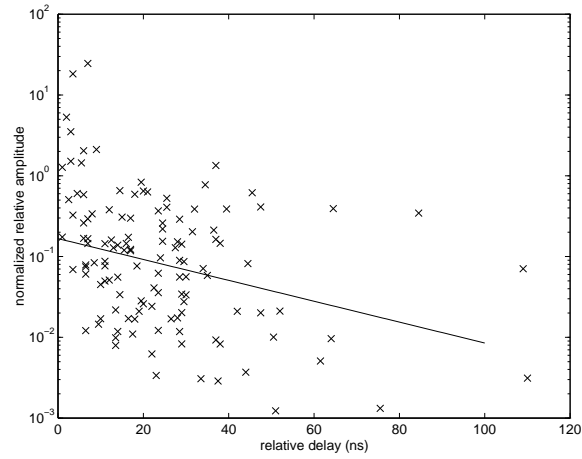


Fig. 7. Plot of normalized cluster amplitude vs. relative delay for the CB, with the curve for $\Gamma = 33.6$ ns superimposed.

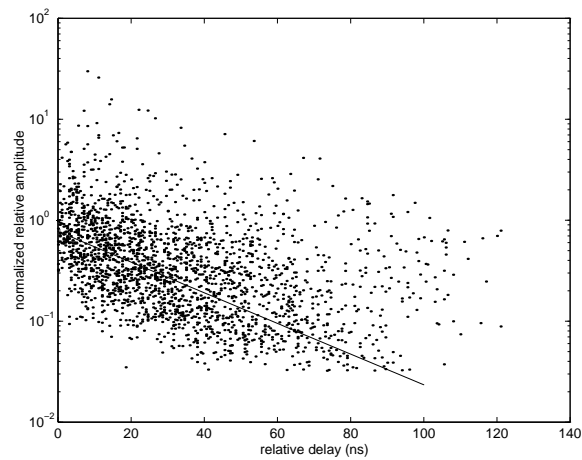


Fig. 8. Plot of normalized ray amplitude vs. relative delay for the CB, with the curve for $\gamma = 28.6$ ns superimposed.

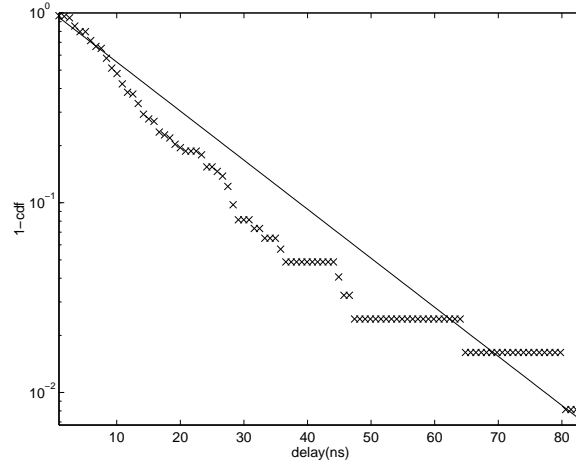


Fig. 9. CDF of Relative Cluster Arrival Times for the CB ($1/\Lambda = 16.8$ ns).

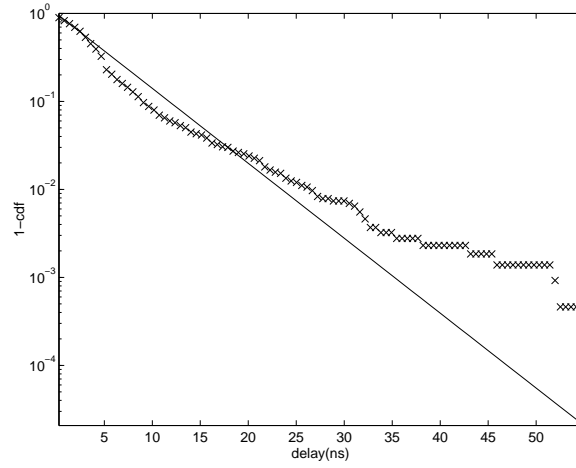


Fig. 10. CDF of Relative Arrival Times Within Clusters in the CB ($1/\lambda = 5.1$ ns).

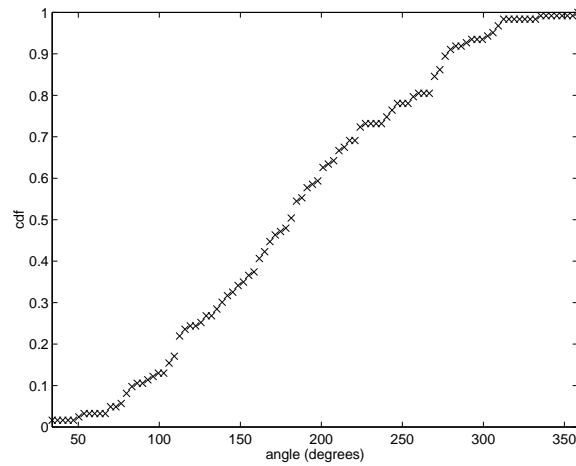


Fig. 11. CDF of relative mean cluster angles in the CB with respect to the first cluster in each set.

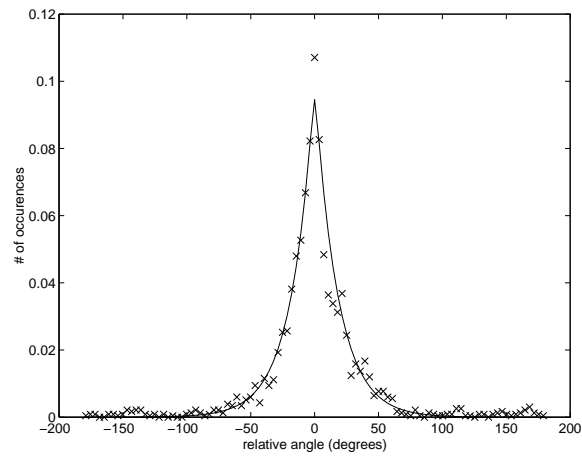


Fig. 12. Histogram of relative ray arrivals with respect to the cluster mean for the CB. Superimposed is the best fit Laplacian distribution ($\sigma = 25.5^\circ$).